**World Scientific**
www.worldscientific.com

# Three-dimensional quantification of protoporphyrin IX in photodynamic therapy using SFDI/DFT: A pilot experimental validation

Mai Dan[*], Weijie Song[†], Meihui Liu[*], Yaru Zhang[*] and Feng Gao[*,‡,§]

[*]*College of Precision Instrument and Optoelectronics Engineering*
*Tianjin University Tianjin 300072, P. R. China*

[†]*Tianjin Medical University Cancer Institute and Hospital*
*Tianjin 300000, P. R. China*

[‡]*Tianjin Key Laboratory of Biomedical Detecting Techniques and Instruments*
*Tianjin 300072, P. R. China*
[§]*gaofeng@tju.edu.cn*

Photodynamic therapy (PDT) dosimetry, including light dose, photosensitizer dose and tissue oxygen, has been a research focus in PDT. In this work, we present a three-dimensional (3D) quantification of protoporphyrin IX (PpIX) using combined spatial frequency domain imaging (SFDI) and diffuse fluorescence tomography (DFT). The SFDI maps both the distributions of tissue absorption and scattering properties at three wavelengths and accordingly provides the optical background for DFT and extracts the tissue oxygenation for assessing the therapeutic outcomes, while DFT dynamically monitors the 3D distribution of PpIX dose from measured fluorescence signals for the procedure optimization. A pilot *in vivo* application in tumor nude models showed that the proposed SFDI/DFT is able to dynamically trace changes in the PpIX concentration and tissue oxygen during the treatment, rendering it a potentially powerful tool for PDT to improve clinical efficacy.

*Keywords*: Photodynamic therapy; spatial frequency domain imaging; diffuse fluorescence tomography.

## 1. Introduction

Photodynamic therapy (PDT) uses the photochemical reactions of photosensitizers to produce cytotoxic products inside tissues that damage biomolecules including proteins and lipids, leading to cancer cell destruction and death.[1] PDT has been widely used in clinical practice for its therapeutic effect on many kinds of tumors.[2,3]

To achieve therapeutic purposes, tumors enriched with photosensitizers are typically irradiated

with light of a specific wavelength. The clinical PDT protocols rely on an empirical given of photosensitizer dose and light dose according to the patient's weight and tumor size but do not take into account the individual differences. In fact, the penetration of light through the target tissue is dependent on the tissue absorption and scattering properties.[4] The heterogeneous distributions of photosensitizer concentration and tissue oxygenation among different individuals and sites also affect the treatment outcomes.[5–7] Therefore, PDT dosimetry, including light dose, photosensitizer dose and tissue oxygen, is of great significance to improve clinical efficacy and has been a research focus in PDT.[8–11]

Recently, spatial frequency domain imaging (SFDI) has received extensive attention in PDT dosimetry due to its advantages of fast, noninvasive and wide field imaging.[12–19] SFDI is an optical imaging modality that enables mapping of the tissue optical properties, including the absorption coefficient ($\mu_a$) and reduced scattering coefficient ($\mu_s'$), by measuring the diffuse reflectances of turbid media at different spatial frequencies.[12] It is also capable of quantitative determination of photosensitizer dose by measuring the fluorescence signals emitted by photosensitizers.[13] Saager *et al.* use SFDI to determine the tissue optical properties in PDT for skin cancer and on this basis report quantitative fluorescence imaging of protoporphyrin IX (PpIX).[14,15] Sunar *et al.* demonstrate that SFDI enables noninvasive determination of PpIX distribution and effect assessment of PDT in nonmelanoma skin cancers.[16–18] However, most of these methods only reconstruct the two-dimensional (2D) images of the optical properties or the photosensitizer dose. At present, no investigation is reported on *in vivo* assessment of PDT that quantifies the dynamic changes in the photosensitizer dose using SFDI.

In this work, we present a three-dimensional (3D) quantification of PpIX-PDT using combined SFDI and diffuse fluorescence tomography (DFT). The SFDI maps both the distributions of tissue absorption and scattering properties at three wavelengths and accordingly offers the priors of the background optical properties for DFT and compares the tissue oxygenations before and after PDT for assessment of the therapeutic outcomes, while DFT dynamically monitors the 3D distribution of PpIX dose from measured fluorescence signals for the procedure optimization. We performed a pilot

*in vivo* validation in tumor nude models. The results showed that the proposed SFDI/DFT is able to dynamically trace changes in the PpIX concentration and tissue oxygen during the treatment, rendering it a potentially powerful tool for PDT to improve clinical efficacy.

## 2. Materials and Methods

### 2.1. *Animal models and experimental preparations*

The protocols and handling of the animals had been approved by Tianjin University Ethics Committee. The mice were acquired from Tianjin Medical university cancer institute and hospital. These nude mice (BALB/c, Charles River) with 4–5 weeks of age had breast cancer cells (4T1) subcutaneously inoculated with $5 \times 10^6$ cell/200 ul in their groin areas. The growing tumors are located shallow beneath the skin, making them easy to observe and measure. 5-aminolevulinic acid (5-ALA) was used as a photosensitizer. When exogenous 5-ALA enters tissues, it can be selectively absorbed by tumor cells, resulting in excessive accumulation of PpIX in tumor. When irradiated by red light, the PpIX produces large amounts of singlet oxygen to damage cancer cells.[5]

Before the treatment, topical application of 5-ALA was adopted for PpIX accumulation. The 5-ALA-hydrochloride (A924477, Macklin) was dissolved in the injection to make a 20% 5-ALA solution. The solution was applied to the tumors with a clean cotton ball for three hours until fully absorbed. The tumors were then treated with a 630 nm laser. Light fractionation PDT is adopted to avoid the rapid depletion of oxygen in tissues (a five minutes interval for every 25 min of irradiation).[20] The radiant exposure is 108 J/cm$^2$ at the irradiance of 12 mW/cm$^2$.[21] A total of six mice were used, five of them as a treatment group and one (mouse #4) as a control group. The control group was also applied with the ALA solution, but exposed to dark environment without irradiation.

### 2.2. *Imaging system and data acquisition*

We utilize a custom-developed SFDI system for data acquisition. The setup of the imaging system is shown in Fig. 1. The light source includes three laser
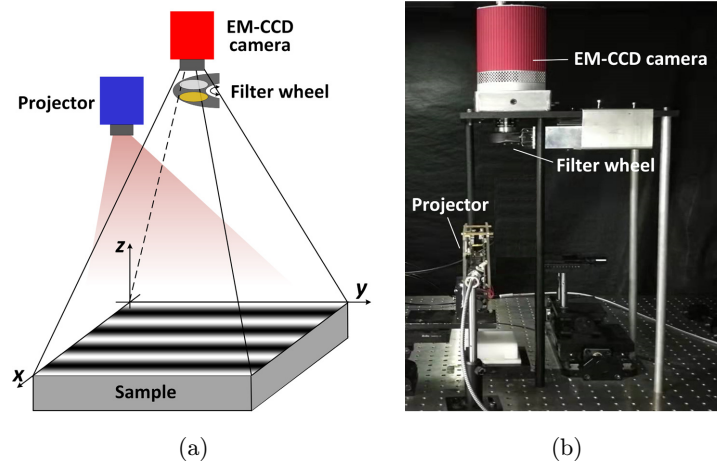
Fig. 1.  SFDI system used in this work. (a) Schematic diagram and (b) photograph.

diodes with the wavelength of 405, 520 and 630 nm, where the 405 nm and 630 nm are the excitation and fluorescence wavelengths of PpIX, respectively. Because the main absorption peak of PpIX is 405 nm with the central wavelength of PpIX fluorescence being 630 nm, the 405 nm excitation can maximize the excitation efficacy. The light source power is >100 mW to ensure the excitation depth. The tissue absorption and scattering properties at these wavelengths are measured to provide the optical background for DFT and to obtain tissue oxygenation. Light from the three laser diodes is coupled into a projector (DlpVisionFly4500, Texas Instruments) through a multimode optical fiber to generate the wild-field sinusoidal illumination. The spatial frequency used is 0.1 mm$^{-1}$. The reflected image or the fluorescence image on tissue surface is

captured using an electron multiplier CCD (EM-CCD) camera (Rolera-MGi, Teledyne Photometrics). A long-pass filter above 600 nm (FEL0600, Thorlabs), controlled through a filter wheel (FW102C, Thorlabs), is used in the fluorescence measurements to filter out the excitation light.

The processes of the treatment and data acquisition are shown in Fig. 2. Before applying the photosensitizers to the tumors, the 3D height maps of mice are first measured using the phase profilometry technique. The height data is used to provide geometric models for DFT and mitigate the surface profile effects of tissues on the optical property extraction. After applying the photosensitizers, the tissue optical properties are measured before and after the treatment. The results at the excitation and fluorescence wavelengths before the treatment
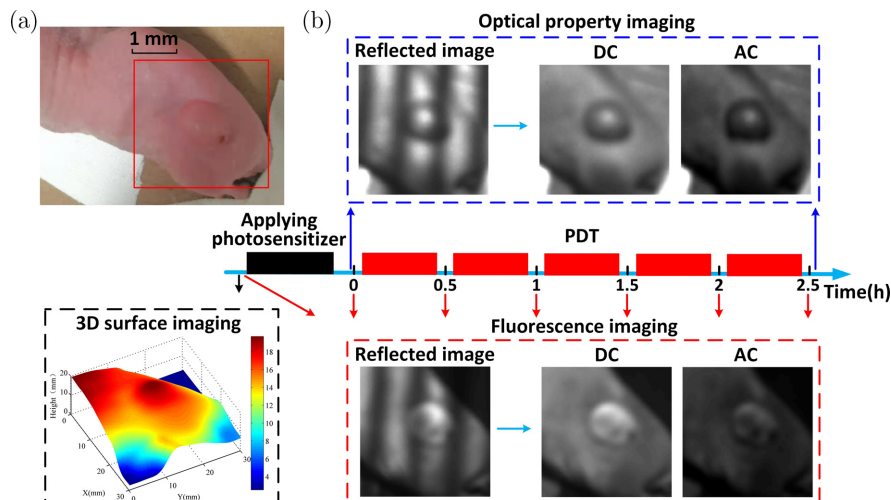


Fig. 2.  The experimental setup. (a) The imaging field of view and (b) the processes of the treatment and data acquisition.

are used as the optical background in DFT to eliminate their effects on measured fluorescence signals. The accordingly extracted tissue oxygenations before and after the treatment are used to assess the PDT outcomes. The fluorescence image is then measured at each interval of the irradiation and used as the input to DFT for dynamically monitoring the 3D distribution of PpIX dose during the treatment. The autofluorescence of mice is also measured as a reference of the fluorescence signal. The planar (DC) and spatially modulated (AC) amplitudes of the images are extracted by projecting three sinusoidal patterns with phase offsets of 0, $2\pi/3$ and $4\pi/3$. All measurements are carried out in a dark environment. The mice were anesthetized and attached to an imaging platform to prevent motion artifacts during the measurements. The pixel resolution of the measured image is $128 \times 128$, with the imaging field of view of $30 \times 30\,\mathrm{mm}^2$. A homogeneous planar phantom with the known optical properties is used for diffuse-reflectance calibrations.

## 2.3. *Quantification of optical properties and PpIX*

The 2D tissue absorption and scattering properties are extracted from the measured diffuse reflectances using a look-up table approach.[9] In order to compensate for the intensity deviations incident onto and reflected from the tissue surface, the DC and AC amplitudes are processed using a correction method.[22] The concentrations of oxyhemoglobin and deoxyhemoglobin, the main absorbers of tissues in visible spectrum, are then determined from the absorption coefficients at the two wavelengths. The extinction coefficients of oxyhemoglobin and deoxyhemoglobin are obtained from an online reference.[23]

The 3D quantification of PpIX is achieved using the spatial frequency domain DFT (SFD-DFT) method. The PpIX dose is characterized using the fluorescence yield which is proportional to the concentration. The forward SFD-DFT model for predicting the excitation and fluorescence flux inside tissues, given the background optical properties and the light source, can be described as a set of diffusion equations.[24] Due to the phase shift of the spatially modulated light source in a heterogeneous medium, the AC response contains both amplitude and phase components and the equations should be expressed in phasor form, referred to as phasor diffusion equations. The 3D distributions of the tissue absorption and scattering properties at the excitation and fluorescence wavelengths are obtained by uniformly assigning the 2D results in the depth direction. The SFD-DFT inverse formulation can be derived in terms of the phasor diffusion equations, within framework of the Born normalization[25]

$$\frac{I_v^{(e)}(\xi_d)}{I_v^{(x)}(\xi_d)}\Gamma_v^{(x)}(\xi_d) = \int_{\Omega_\mathrm{r}} G_v^{(e)}(\xi_d, \mathbf{r})\Phi_v^{(x)}(\mathbf{r})\beta(\mathbf{r})d\mathbf{r}, \quad (1)$$

where $I_v^{(e)}(\xi_d)$ and $I_v^{(x)}(\xi_d)$ denote the measured modulation amplitudes of the fluorescence ($e$) and excitation ($x$) wavelengths at the detection position, $\xi_d$, on tissue surface, with $v \in \{\mathrm{DC, AC}\}$ denoting the DC and AC; $\Gamma_v^{(x)}(\xi_d)$ represents the light flow of the excitation on tissue surface; $\Omega_\mathbf{r}$ is the domain of integration; $\Phi_v^{(x)}(\mathbf{r})$ and $\beta(\mathbf{r})$ represent the light flux phasor and fluorescence yield at the position $\mathbf{r}$ inside the tissue, respectively; $G_v^{(e)}(\xi_d, \mathbf{r})$ represents the Green's function. The $\Gamma_v^{(x)}(\xi_d)$, $\Phi_v^{(x)}(\mathbf{r})$ and $G_v^{(e)}(\xi_d, \mathbf{r})$ are calculated on basis of the forward model and the Robin boundary condition.[26] To solve the forward model, we build the 3D complex geometry of each mouse from the measured height data and solve it with finite element method.[27]

The above equation can be discretized into the following matrix notation:

$$\mathbf{Y} = \mathbf{J}\boldsymbol{\beta}, \quad (2)$$

where $\mathbf{Y}$ is the Born-normalized data, $\mathbf{J}$ is the Jacobian matrix regarding the Born normalization and $\boldsymbol{\beta}$ represents the fluorescence yields at the finite element nodes. The matrix equation is solved using the algebraic reconstruction technique.[28]

## 3. Results

We first showed the 2D maps of the optical properties and tissue oxygen saturation ($\mathrm{StO}_2$) and compared their changes before and after the treatment. The results of DFT were then shown to reflect the PpIX dose inside tissues, with the distribution concentrated at the edge of the tumor within the depth of $1.5\,\mathrm{mm}$ beneath the surface. Finally, we investigated the temporal variation of PpIX dose

during the treatment and discussed the effects of PpIX and $StO_2$ decreases on PDT outcomes.

### 3.1.   *Maps of optical properties and $StO_2$*

Figure 3 shows the optical property maps of mouse #2 at the two wavelengths before the treatment. The $\mu_a$ was slightly higher in tumors than that in normal tissues, while the $\mu_s'$ did not show significant differences between them. Due to the large surface curvatures in tumor edges, the correction method failed to completely compensate for the diffuse reflectance deviations, leading to the biased optical properties in these regions, as shown in the zoomed-in versions. Since only a single course of PDT was performed in the experiment and the light dose was

low, no significant changes in tumor size were observed after the treatment.

The changes in the $\mu_a$ before and after the treatment were then analyzed. The means of $\mu_a$ in tumors at 405 nm and 520 nm increased slightly after the treatment, while the means at 630 nm slightly decreased. The results showed good consistence among the mice in the treatment group. The changes in $\mu_a$ may result from the changes in tissue oxygenation such as the total hemoglobin concentration and $StO_2$. We calculated the $StO_2$ from the $\mu_a$ at the wavelengths of 520 nm and 630 nm. The results are shown in Fig. 4. A slight decrease in $StO_2$ was observed in most mice. Oxygen consumption caused by the photochemical reactions may be the major reason for the decreases of $StO_2$ in the
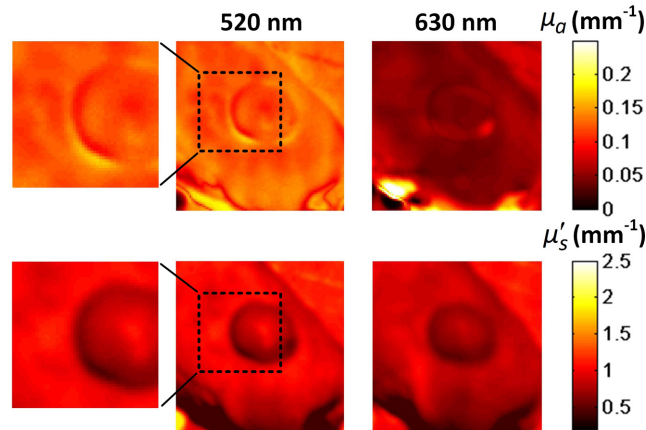


Fig. 3.   Optical absorption and scattering maps of mouse #2 before the treatment at the wavelengths of 520 nm and 630 nm.
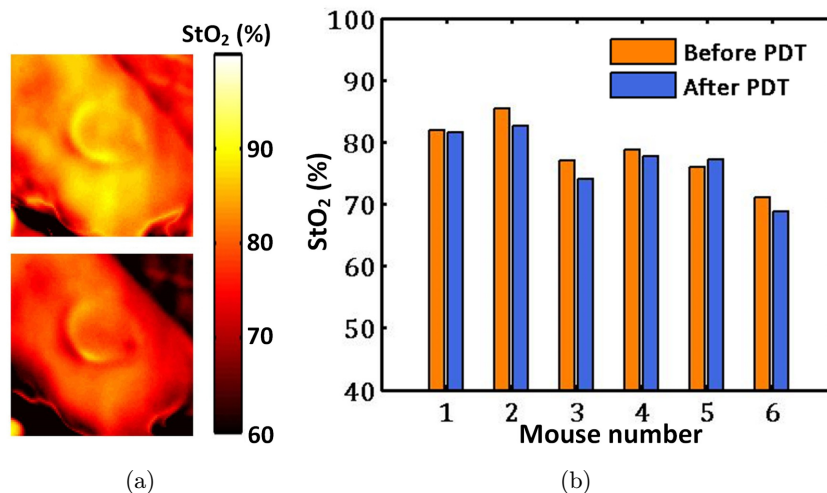


(a)
(b)

Fig. 4.   Results of $StO_2$. (a) The $StO_2$ maps of mouse #2 before (top) and after (blow) the treatment; (b) mean $StO_2$ values in tumors before and after the treatment. Mouse #4 is the control group.

tumors. The $StO_2$ in the control group and normal tissues also decreased after the treatment, which was probably caused by prolonged anesthesia.

## 3.2. 3D quantification of PpIX

Finally, we reconstructed the 3D distribution of PpIX fluorescence yield using the SFD-DFT method described in Sec. 2.3. The geometry of the mice is discretized with tetrahedron elements containing about 60,000 nodes. The fluorescence yields at the finite element nodes are linearly interpolated to produce the map with resolution of $128 \times 128$ at different depths. To better represent the tomographic results, we plotted the top views of the fluorescence yields at different depths beneath the mouse surface. In addition, the sections in the X–Z and Y–Z directions are also presented to show the surface profiles.

Figure 5 shows the results of mouse #2. Before the treatment, the fluorescence yields in the tumors were significantly higher than those in the normal tissues. The results indicated that the ALA solution was selectively absorbed by the tumor cells and metabolized to produce the PpIX that enriched the tumors. The normal tissues also had a small concentration of PpIX, which probably resulted from blood transport and metabolism. From the depth direction, the PpIX was mainly distributed within the depth of 0–1.5 mm beneath the surface and concentrated at the edges of the tumors, with the dose decreased rapidly at the deeper tissues, as shown in Fig. 5(c). The limited penetration depth of photosensitizers through percutaneous delivery may

account for the superficial distribution of PpIX. In addition, the limited penetration depth of the excitation light inside the tissues can result in the failure of PpIX in the deeper positions to stimulate and release fluorescence. After the treatment, the concentration of PpIX was reduced in both the tumors and normal tissues, as shown in Fig. 5(b). The depletion by the photodynamic reactions may be an important cause to the decreased PpIX concentration, which can explain the greater decline in the tumors than in normal tissues. Besides, the tissue metabolism of photosensitizers also reduces the concentration (usually metabolized completely in 24 h).

Figure 6 shows the average fluorescence yields versus time. The areas of the tumors and normal tissues used for calculating the mean values are indicated in Fig. 5(b). The depth of the two areas is within 2 mm. The origin of the time axis corresponds to the measurements taken before the treatment. The autofluorescence of mice before applying the photosensitizers ($-0.5$ h) was also calculated. Due to the individual differences in drug uptake, the PpIX dose in each mouse is significantly different. Though the temporal variation of the PpIX concentration had good consistency among mice. In the treatment group, the concentrations of the PpIX in the tumors reached the highest level after applying the photosensitizers and gradually decreased with the treatment, reaching about half of the initial values after 2.5 h. Specifically, the concentrations decreased rapidly during the first hour and slowed down afterwards. In the control group, the concentrations of the PpIX remained
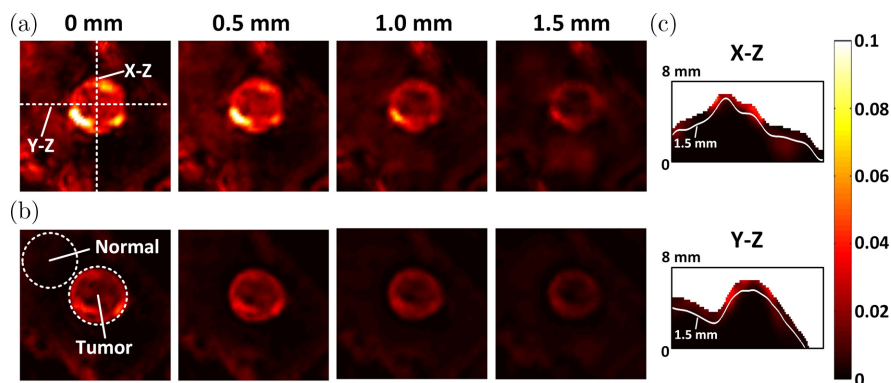


Fig. 5. Tomographic reconstructions of PpIX fluorescence yields of mouse #2. Fluorescence yield maps at different depths (a) before and (b) after the treatment; (c) sections of the fluorescence yields before the treatment in X–Z and Y–Z directions. The dotted lines and circles indicate the positions of the sections and the areas of the tumor and normal tissues used to calculate the average fluorescence yields, respectively.
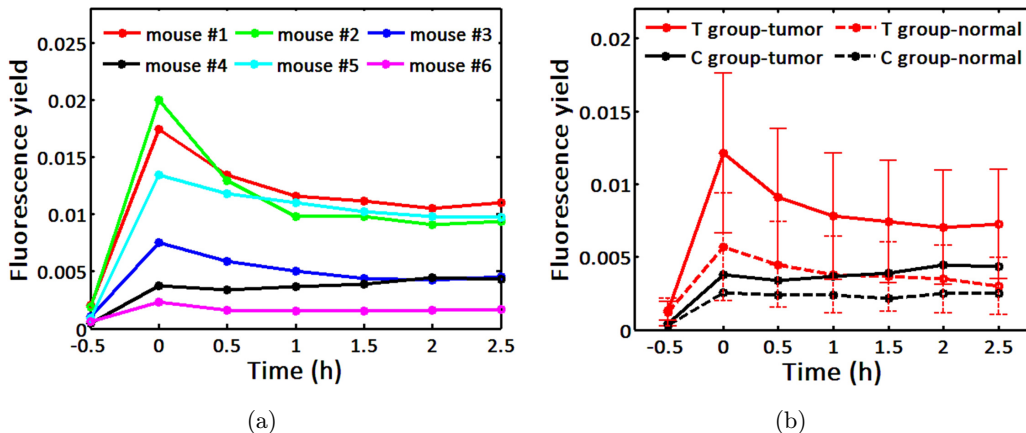
Fig. 6.   PpIX fluorescence yields versus time. (a) Results in tumors; (b) results in tumors and normal tissues between the treatment (T) and control (C) groups. The error bars in the T group indicate the standard deviations for the tumors (solid lines) and normal tissues (dotted lines).

at the same level, with no decreasing trend. Figure 6(b) shows the fluorescence yields of the tumors and normal tissues versus time in the treatment group and the control group. The curves of the treatment group are obtained by calculating the average fluorescence yields of five mice. The temporal variation of the PpIX concentration shows significant differences between the two groups and between the tumors and normal tissues.

Above results indicate that there are significant differences among individuals in the spatial distribution and temporal variation of PpIX dose as well as in the optical properties and tissue oxygenation. We also noted a correlation of tumor growth to both PpIX concentration and tissue oxygenation. As tumors grew, the $StO_2$ and PpIX concentrations of mice appeared to decrease (The mice with larger numbers had longer tumor growth time when measured, e.g., the tumor of mouse #6 grew nearly five days longer than that of mouse #1.). It is speculated that the growth of tumors impaired the physiological function of the mice, leading to the decrease in tissue oxygen and drug absorption. Since the efficacy of PDT is dependent on concentration of the singlet oxygen produced in tissues, which is proportional to the product of local photosensitizer dose and light dose in simple case,[7] the decreases of PpIX dose and oxygen can result in reduced treatment outcomes.

## 4.   Discussions and Conclusion

This work has achieved the quantification of PpIX dose and tissue oxygenation. The light dose can also be predicted from the diffusion equation. Therefore, the concentration of singlet oxygen is able to be estimated during the treatment. The ultimate goal of this study is to provide guidance for treatment optimization, including the additional application of photosensitizers or local increases in light irradiance, to compensate for the PpIX dose and oxygen depletions during the treatment. Due to the small number of mice measured in the experiment and the lack of long-term monitoring of tumors for assessment of the therapeutic outcomes, more works are required to further verify the clinical performance of the method. But existing results have proved that the method provides a feasible strategy for PDT dosimetry. Despite the success, there are limitations of the proposed method that require to be discussed.

In this work, the 405 nm excitation is adopted. Despite that the 405 nm excitation can maximize the excitation efficacy of PpIX fluorescence, its excitation depth is limited. We have validated the effective penetration depths of the excitation light using the Monte Carlo simulation and found that the values are less than 1 mm and 0.7 mm at the DC and $0.1\,\text{mm}^{-1}$, respectively. Compared to the superficial fluorescence, the fluorescence beneath the penetration depth is very weak. Successful detection of these weak fluorescence signals requires a high-power light source to enhance the excited fluorescence intensity and a high-sensitivity detector to capture them escaping from the surface. Considering the high excitation efficacy at 405 nm, the use of a high-power excitation source combined with a high-sensitivity EM-CCD camera can detect the fluorescence beneath 1 mm. This depth may be

sufficient for this study as the topical application of ALA normally has superficial distribution, but it can be very limited for tomography of deeper tumors. The 630 nm excitation of PpIX will be used as the alternative strategy in further work, which has greater advantages in the excitation depth.[19]

We obtain the tissue oxygenation from the absorption coefficients at the 520 nm and 630 nm. But the two wavelengths have different penetration depths, which differ by approximately 0.5 mm at the measured optical properties. The differences in the penetration depth can reduce the accuracy of the obtained tissue oxygenation as the main chromophores, including hemoglobin, melanin and fat are distributed at different depths inside the tissues. More works are required in the future to improve the results of tissue oxygenation. These works include using the wavelength near 630 nm to reduce the difference in the penetration depth and studying the method for depth-resolved quantitation of optical properties to distinguish the absorption contributions of hemoglobin from those of other chromophores inside the tissues.

The surface issue has been a challenge for SFDI. The surface heights and curvatures affect both the measured light intensity and spatial frequencies. To mitigate the surface effects on the reconstructions, we measure the surface profile of each mouse and adopt the profile-based Minnaert's correction and the multi-frequency processing and interpolation methods to compensate for the intensity and spatial frequency deviations, respectively. The corrections work well for low-angle areas but do not function effectively for tumor edges with large heterogeneities and surface curvatures. The results are mainly caused by the following limitations. First, the Minnaert's correction method assumes that the measured reflectances of low-angle areas are representative of the entire region and large heterogeneities are likely to introduce errors. Second, the frequency interpolation method requires the real spatial frequency projected, which is difficult to obtain for steep surfaces. In addition to the correction methods, the errors also result from the height data. In this work, we measured the mice surfaces only at the beginning of the experiment and assumed that the surfaces are unchanged. However, the movement of the mice during the experiment can cause their real positions and postures to be inconsistent with the measurements, which accordingly can reduce the correction performance.

In future works, more effective correction methods and the profilometry techniques with enhanced performances in both accuracy and speed are required to handle the surface issue.

In addition, we have observed that the reconstructed PpIX fluorescence yield are inflated at the depth of 1–2 mm. In fact, the topical application of ALA normally does not go deeper than 1 mm *via* diffusion. The errors in the results may be caused by the following reasons: First, the diffuse model can be inappropriate for predicting the light flux at the excitation light due to the high tissue-absorption properties. Compared to the Monte Carlo simulations, the diffusion model solutions are numerically biased by about 15% at the measured optical properties and spatial frequencies. The errors can be partly reduced in the framework of the Born normalization due to the ratio relationship between the light flow and light flux, but it can still lead to the reduced accuracy in the DFT reconstruction. In future work, we will consider using more accurate forward model, such as Monte Carlo simulation, for the reconstructions. Second, the uniform assignment of the optical properties to provide the 3D optical background can also cause errors to the reconstructions as the tissues normally have the layered structures. Our recent work is to study the method for depth-resolved quantitation of optical properties in layered media, which is expected to provide the more accurate optical background for DFT. Third, the errors can also result from the mesh dissections in the finite element method. In this work, the geometry is subdivided into tetrahedral elements following a gradual coarsening from the surface downwards. This meshing strategy can improve the reconstruction efficiency, but it can cause the spatial resolution of the results to decrease with the depth. The linear interpolation of the results therefore leads to greater errors as the depth increases. Finer meshing can reduce such errors, but the resulting increase in node numbers will bring the increased ill-posedness and computational burden for solving the inverse problems.

In this work, the algebraic reconstruction technique is used for solving the inverse problem, which has strong performance in robustness and convergence. For the class of inverse problems in this study, it can obtain a minimum norm solution. Appropriate regularization method, such as Tikhonov regularization, can help accelerate the convergence and improve the accuracy of the solution. But the

regularization requires prior knowledge, otherwise it may cause subjective errors. In this work, the depth regularization is inherent to the measurements as the penetration depth varies at each spatial frequency, therefore the use of multi-frequency measurements can mitigate the skin effect in the results. Beyond that, no additional regularization is used to constrain the solution. Future work will focus on the data-driven adaptive regularization methods or deep learning methods to further improve the solution. To mitigate the surface contributions, we build the 3D complex geometry for each mouse based on the measured surface data. The curved boundaries of the geometries match the real surfaces, which therefore can mitigate the surface contributions on the reconstructions. In addition, a pair of linear polarizers is used in the imaging system to eliminate the specular reflections from the surface.

In summary, this work presents a 3D quantification of PpIX in PDT using combined SFDI and DFT. The scheme first maps both the distributions of tissue absorption and scattering properties to provide the optical background for DFT and accordingly extracts tissue oxygenation for the assessment of PDT outcomes and finally monitors the 3D distribution of PpIX concentration for procedure optimization. The pilot *in vivo* application in tumor nude models demonstrated the feasibility of the proposed SFDI/DFT to dynamically trace changes in the PpIX concentration and tissue oxygen during the treatment. This method is expected to provide guidance for the individualization of PDT, including pre-operative planning and intraoperative adjustment, and ultimately improve the treatment outcomes.

## Conflicts of Interest

The authors declare that there are no conflicts of interest relevant to this paper.

## Acknowledgment

## References

1. A. P. Castano, T. N. Demidova, M. R. Hamblin, "Mechanisms in photodynamic therapy: Part one: Photosensitizers, photochemistry and cellular localization," *Photodiagn. Photodyn. Ther.* **1**(4), 279–293 (2004).

2. S. B. Brown, E. A. Brown, I. Walker, "The present and future role of photodynamic therapy in cancer treatment," *Lancet Oncol.* **5**(8), 497–508 (2004).

3. L. M. Chong, D. J. H. Tng, L. L. Y. Tan, M. L. K. Chua, Y. Zhang, "Recent advances in radiation therapy and photodynamic therapy," *Appl. Phys. Rev.* **8**, 041322 (2021).

4. R. R. Allison, K. Moghissi, "Oncologic photodynamic therapy: Clinical strategies that modulate mechanisms of action," *Photodiagn. Photodyn. Ther.* **10**(4), 331–341 (2013).

5. B. C. Wilson, M. S. Patterson, "The physics, biophysics and technology of photodynamic therapy," *Phys. Med. Biol.* **53**, 61–109 (2008).

6. C. M. Gardner, S. L. Jacques, A. J. Welch, "Fluorescence spectroscopy of tissue: recovery of intrinsic fluorescence from measured fluorescence," *Appl. Opt.* **35**(10), 1780–1792 (1996).

7. M. M. Kim, A. A. Ghogare, A. Greer, T. C. Zhu, "On the *in-vivo* photochemical rate parameters for PDT reactive oxygen species modeling," *Phys. Med. Biol.* **62**(5), R1–R48 (2017).

8. B. H. Li, S. S. Xie, Z. Huang, B. C. Wilson, "Advances in photodynamic therapy dosimetry," *Prog. Biochem. Biophys.* **36**(6), 676–683 (2009).

9. A. J. Ruiz, E. P. M. LaRochelle, J. R. Gunn, S. M. Hull, T. Hasan, M. S. Chapman, B. W. Pogue, "Smartphone fluorescence imager for quantitative dosimetry of protoporphyrin-IX-based photodynamic therapy in skin," *J. Biomed. Opt.* **25**(6), 063802 (2019).

10. M. Mousavi, L. T. Moriyama, C. Grecco, M. S. Nogueira, K. Svanberg, C. Kurachi, S. A. Engels, "Photodynamic therapy dosimetry using multi-excitation multiemission wavelength: Toward real-time prediction of treatment outcome," *J. Biomed. Opt.* **25**(6), 063812 (2020).

11. T. J. Moritz, Y. B. Zhao, M. F. Hinds, J. R. Gunn, J. R. Shell, B. W. Pogue, S. J. Davis, "Multispectral singlet oxygen and photosensitizer luminescence dosimeter for continuous photodynamic therapy dose assessment during treatment," *J. Biomed. Opt.* **25**(6), 063810 (2020).

12. D. J. Cuccia, F. Bevilacqua, A. J. Durkin, F. R. Ayers, B. J. Tromberg, "Quantitation and mapping of tissue optical properties using modulated imaging," *J. Biomed. Opt.* **14**(2), 024012 (2009).

13. S. D. Konecky, C. M. Owen, T. Rice, P. A. Valdés, K. Kolste, B. C. Wilson, F. Leblond, D. W. Roberts, K. D. Paulsen, B. J. Tromberg, "Spatial frequency domain tomography of protoporphyrin IX

fluorescence in preclinical glioma models," *J. Biomed. Opt.* **17**(5), 056008 (2012).

14. R. B. Saager, D. J. Cuccia, A. J. Durkin, "Determination of optical properties of turbid media spanning visible and near-infrared regimes via spatially modulated quantitative spectroscopy," *J. Biomed. Opt.* **15**, 017012 (2010).

15. R. B. Saager, D. J. Cuccia, S. D. Saggese, K. M. Kelly, A. J. Durkin, "Quantitative fluorescence imaging of protoporphyrin IX through determination of tissue optical properties in the spatial frequency domain," *J. Biomed. Opt.* **16**, 126013 (2011).

16. U. Sunar, D. J. Rohrbach, J. Morgan, N. Zeitouni, B. W. Henderson, "Quantification of PpIX concentration in basal cell carcinoma and squamous cell carcinoma models using spatial frequency domain imaging," *Biomed. Opt. Exp.* **4**, 531–537 (2013).

17. D. J. Rohrbach, D. Muffoletto, J. Huihui, R. Saager, K. Keymel, A. Paquette, J. Morgan, N. Zeitouni, U. Sunar, "Preoperative mapping of nonmelanoma skin cancer using spatial frequency domain and ultrasound imaging," *Acad. Radiol.* **21**(2), 263–270 (2014).

18. D. J. Rohrbach, N. C. Zeitouni, D. Muffoletto, R. Saager, B. J. Tromberg, U. Sunar, "Characterization of nonmelanoma skin cancer for light therapy using spatial frequency domain imaging," *Biomed. Opt. Exp.* **6**, 1761–1766 (2015).

19. D. J. Wirth, M. Sibai, B. C. Wilson, D. W. Roberts, K. Paulsen, "First experience with spatial frequency domain imaging and red-light excitation of protoporphyrin IX fluorescence during tumor resection," *Biomed. Opt. Exp.* **11**(8), 4306–4315 (2020).

20. C. Framme, B. Flucke, R. Birngruber, "Comparison of reduced and standard light application in photodynamic therapy of the eye in two rabbit models," *Graefes Arch. Clin. Exp. Ophthalmol.* **244** (7), 773–781 (2006).

21. B. W. Henderson, T. M. Busch, J. W. Snyder, "Fluence rate as a modulator of PDT mechanisms," *Lasers Surg. Med.* **38**(5), 489–493 (2006).

22. M. Dan, M. H. Liu, W. X. Bai, F. Gao, "Profile-based intensity and frequency corrections for single-snapshot spatial frequency domain imaging," *Opt. Exp.* **29**(9), 12833–12848 (2021).

23. S. Prahl, Assorted Spectra, https://omlc.org/spectra/.

24. S. C. Davis, D. Hamid, W. Jia, S. D. Jiang, B. W. Pogue, K. D. Paulsen, "Image-guided diffuse optical fluorescence tomography implemented with Laplacian-type regularization," *Opt. Exp.* **15**(7), 4066–4082 (2007).

25. A. Soubret, J. Ripoll, V. Ntziachristos, "Accuracy of fluorescent tomography in the presence of heterogeneities: study of the normalized Born ratio," *IEEE Trans. Med.* **24**(10), 1377–1386 (2005).

26. V. A. Markel, J. C. Schotland, "Inverse problem in optical diffusion tomography. II. Role of boundary conditions," *J. Opt. Soc. Am. A* **19**(3), 558–566 (2002).

27. S. R. Arridge, M. Schweiger, M. Hiraoka, D. T. Delpy, "A finite element approach for modeling photon transport in tissue," *Med. Phys.* **20**(2), 299–309 (1993).

28. X. Intes, V. Ntziachristos, J. P. Culver, A. Yodh, B. Chance, "Projection access order in algebraic reconstruction technology for diffuse optical tomography," *Phys. Med. Biol.* **47**, 1–10 (2002).